



OPEN ACCESS

EDITED BY

Lawrence Miller,
University of Illinois at Chicago,
United States

REVIEWED BY

Albano Neto Carneiro Neto,
University of Aveiro, Portugal
Ricardo Luiz Longo,
Federal Rural University of Pernambuco,
Brazil

*CORRESPONDENCE

Miki Hasegawa,
hasemiki@chem.aoyama.ac.jp

SPECIALTY SECTION

This article was submitted to Inorganic Chemistry, a section of the journal Frontiers in Chemistry

RECEIVED 19 September 2022

ACCEPTED 09 November 2022

PUBLISHED 07 December 2022

CITATION

Ohmagari H, Marets N, Kamata J, Yoneyama M, Miyauchi T, Takahashi Y, Yamamoto Y, Ogihara Y, Saito D, Goto K, Ishii A, Kato M and Hasegawa M (2022), Thermosensitive visible-light-excited visible-/NIR-luminescent complexes with lanthanide sensitized by the π -electronic system through intramolecular H-bonding. *Front. Chem.* 10:1047960. doi: 10.3389/fchem.2022.1047960

COPYRIGHT

© 2022 Ohmagari, Marets, Kamata, Yoneyama, Miyauchi, Takahashi, Yamamoto, Ogihara, Saito, Goto, Ishii, Kato and Hasegawa. This is an open-access article distributed under the terms of the [Creative Commons Attribution License \(CC BY\)](https://creativecommons.org/licenses/by/4.0/). The use, distribution or reproduction in other forums is permitted, provided the original author(s) and the copyright owner(s) are credited and that the original publication in this journal is cited, in accordance with accepted academic practice. No use, distribution or reproduction is permitted which does not comply with these terms.

Thermosensitive visible-light-excited visible-/NIR-luminescent complexes with lanthanide sensitized by the π -electronic system through intramolecular H-bonding

Hitomi Ohmagari^{1,2}, Nicolas Marets^{1,2}, Jun Kamata¹, Mayo Yoneyama¹, Takumi Miyauchi¹, Yuta Takahashi¹, Yukina Yamamoto¹, Yuto Ogihara¹, Daisuke Saito^{3,4}, Kenta Goto⁵, Ayumi Ishii⁶, Masako Kato⁴ and Miki Hasegawa^{1,2*}

¹Department of Chemistry and Biological Science, Aoyama Gakuin University, Sagami-hara, Japan,

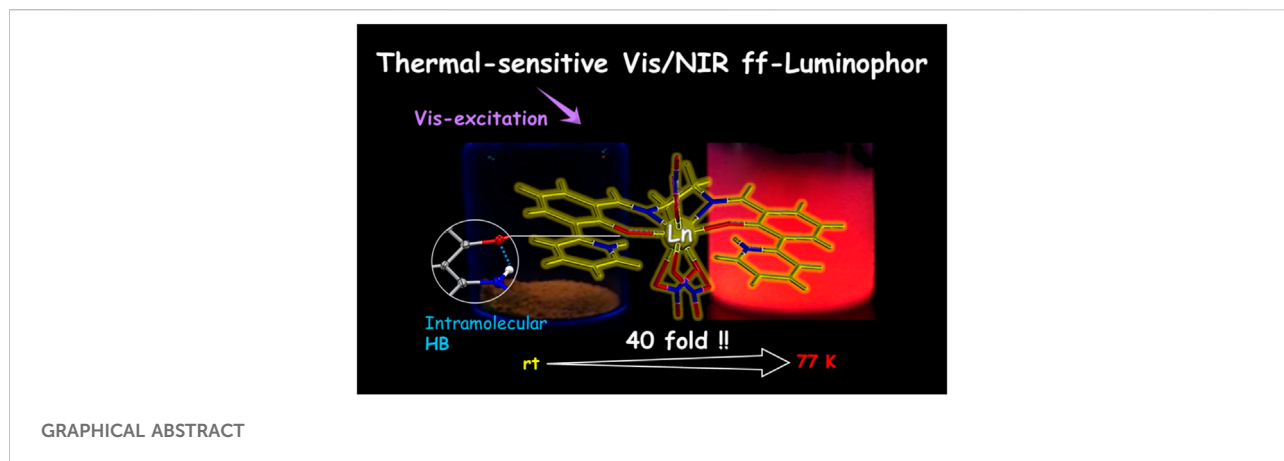
²Mirai Molecular Materials Design Institute, Aoyama Gakuin University, Sagami-hara, Japan,

³Department of Chemistry, Faculty of Science, Hokkaido University, Sapporo, Japan, ⁴Department of Applied Chemistry for Environment, School of Biological and Environmental Sciences, Kwansai Gakuin University, Sanda, Japan, ⁵Institute for Materials Chemistry and Engineering, Kyushu University, Fukuoka, Japan, ⁶Department of Natural and Environmental Science, Teikyo University of Science, Yamanashi, Japan

Visible-luminescent lanthanide (LnL) complexes with a highly planar tetradentate ligand were successfully developed for a visible-light solid-state excitation system. **L** was designed by using two 2-hydroxy-3-(2-pyridinyl)-benzaldehyde molecules bridged by ethylenediamine, which was then coordinated to a series of Ln ions (Ln = Nd, Sm, Eu, Gd, Tb, Dy, and Yb). From the measurement of single-crystal X-ray analysis of Eu**L**, two phenolic O atoms and two imine N atoms in **L** were coordinated to the Eu ion, and each π -electronic system took coplanar with the edged-pyridine moiety through an intramolecular hydrogen bond. The enol group on the phenolic skeleton changed to the keto form, and the pyridine was protonated. Thus, intramolecular proton transfer occurred in **L** after the complexation. Other complexes take isostructure. The space group is *P*-1, and the *c*-axis shrinks with decreasing temperature without a phase transition in Eu**L**. The yellow color caused by the planar structure of **L** can sensitize ff emission by visible light, and the luminescence color of each complex depends on central Ln ions. Furthermore, a phosphorescence band also appeared at rt with ff emission in Ln**L**. Drastic temperature dependence of luminescence was clarified quantitatively.

KEYWORDS

lanthanide complexes, visible-light excitation, visible-/NIR-luminescence, intramolecular H-bonding, thermosensitive luminescence



1 Introduction

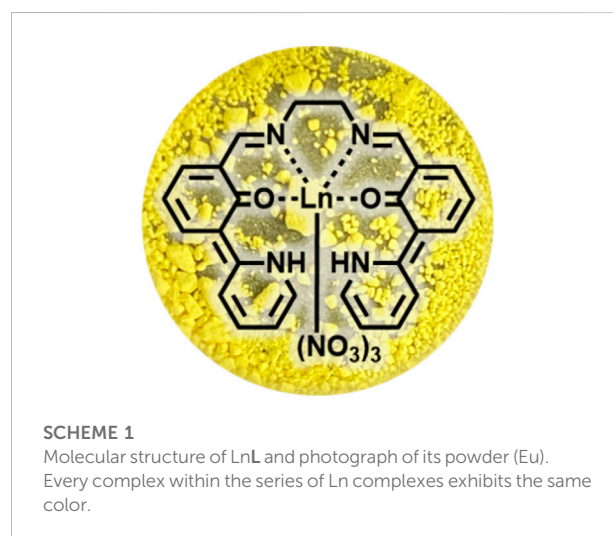
Visible-light-excitable chromophores with visible-/NIR-light emission are very useful in physiological fields, for example, as biosensors, since visible light can prevent damage to cells and the luminescence of colored cells can be detected easily because the transparency of the skin is improved (Bender et al., 2002; Deiters et al., 2009; Jiang et al., 2010; Hasegawa et al., 2014; Ning et al., 2019; Parker et al., 2021). For the luminescence and structure stability in solutions and solid state, metal complexes considering chelate effect have potential. We designed and newly synthesized a tetradentate ligand (L) for a series of visible-light-excitable lanthanide (Ln) complexes with visible-/NIR-luminescence in the solid state (Schemes 1, 2). Ln ions in complexes exhibit characteristic band positions and have relatively long luminescence lifetimes in milliseconds because of their electron configuration. This is related to the parity selection rules (ff transitions), and the narrowness of these transitions is due to the shielding effects (electronic configuration). Therefore, their luminescence has the advantage of being easily distinguishable from other luminescent molecules in the living body. Based on these unique properties, the complex LnL will be a candidate for applications to biological sensing materials. The ligand maintains its complexation with Ln by a chelate effect (Francis et al., 2020; Hasegawa and Ohmagari, 2020).

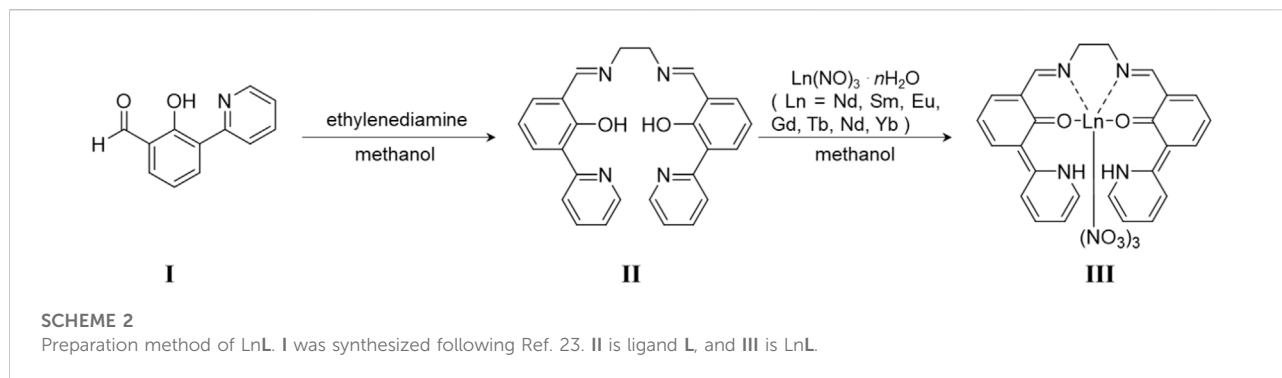
The luminescence color of Ln complexes is derived from Ln³⁺ species, for example, a Eu³⁺ complex shows pure red emission. These unique optical properties are due to the electronic configuration or electronic state for the *f*-orbital of the Ln ion. The band position of ff emissions for trivalent Ln ions depends on the number of *f*-electrons whose energy levels have been decided by the split under some rules such as relative magnitude of the interelectronic repulsion, spin-orbital coupling, and crystal-field effects (Binnemans, 2015).

In the case of Ln ions, the ff electron transitions are not involved in the reference vibration due to the shielding effect of

the 5s and 5p orbitals in the outer shell. Thus, the usual method is to bind aromatic organic molecules with high absorption coefficients as ligands and promote ff emission of Ln through an intramolecular energy transfer *via* photo-excitation. This ff emission sensitization mechanism is known as the photo-antenna effect. However, a suitable excitation wavelength for the energy acceptor level for Ln³⁺, which shows emission in the visible light region, is mostly in the UV region, and there are very few reports on Ln complexes showing visible-light excitation and visible-light luminescence (Werts et al., 1999; Yang et al., 2004; Deun et al., 2005; Zhang et al., 2005; An et al., 2008; Chen et al., 2008; Andreiadis et al., 2009; He et al., 2009; Divya et al., 2010; He et al., 2010; Gu and Yan, 2013; Zhang et al., 2013; Sun et al., 2014; Xu et al., 2014; Aquino et al., 2021; Zhang et al., 2021).

The Eu³⁺ complex with 9-hydroxyphenal-1-one molecules (Deun et al., 2005) forms a highly coplanar π -electronic system, and its absorption band appears in the visible region. Similarly, a series of Eu³⁺ complexes with carbazole (He et al., 2009; He et al., 2010), tetrazole (Andriadis et al., 2009), and β -diketone (Werts





et al., 1999; Divya et al., 2010) also show visible-excitable luminescence due to coplanar π -electronic systems. There are few specific examples for the energy relaxation process in which energy transfer to the center metal occurs *via* not the triplet energy level but a singlet one (Yang et al., 2004; Kasprzycka et al., 2017; Aquino et al., 2021). In particular, the Eu^{3+} complex with a 2,4-di (2-pyridyl)-1,3,5-triazine derivative shows high luminescence quantum yield (QY; φ_L) and $\varphi_L = 0.52$ ($\lambda_{\text{ex}} = 402$ nm) at room temperature (abbreviated to rt). Visible-light-excited luminescent Ln–Ln' complexes based on ff absorption were reported in 1993 by Bünzli et al. (1993). They synthesized dinuclear Eu/Tb–Ln (Ln = Nd, Ho, and Yb) complexes with *p*-tert-butylcalix [8] arene and observed red emission in Eu–Ln excited at the absorption band position of the ${}^7F_0 \rightarrow {}^5D_0$ transition of Eu^{3+} (Bünzli et al., 1993).

In this investigation, we aim to clarify the solid state luminescence properties of a series of LnL (Ln = Nd, Sm, Eu, Gd, Tb, Dy, and Yb) complexes by luminescence QY and lifetime measurement and with a single-crystal X-ray structure analysis and temperature-dependence of synchrotron X-ray diffraction (XRD) patterns for their sophisticated molecular and packing structures.

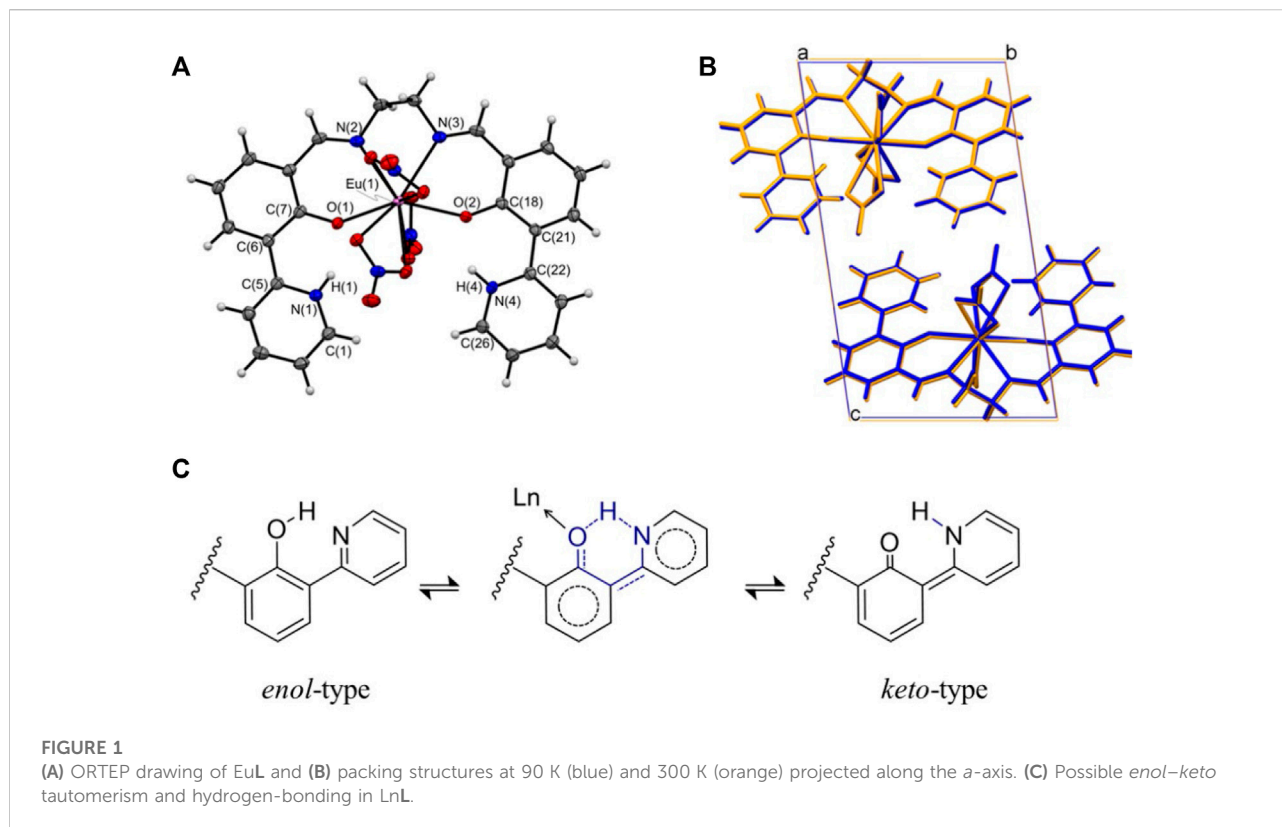
2 Results and discussion

2.1 Single-crystal structural analyses of LnL

A series of LnL complexes were obtained as yellowish crystals, and single-crystal X-ray structure diffraction analysis was performed to determine the molecular structures. In the case of EuL, the molecular structure and an overlay figure showing the packing structure at 90 and 300 K are shown in Figure 1. The crystal data and bond distances are summarized in Supplementary Tables S1, S3. L equatorially coordinates to Eu^{3+} as a tetradentate ligand at ONNO, and three nitrate ions as bidentate bind axially to Eu^{3+} . Focusing on the 2-(pyridine-2-yl)phenol framework in L, intramolecular proton transformation (IPT) occurred before and after complexation, and L

formed an intermediate form between keto and enol (Figure 1C). Actually, the bond lengths for C(7)–O(1) and C(18)–O(2) for the phenol moiety in LnL are almost 1.31 Å, which is the shorter- and longer-value than actual values of 1.38–1.39 Å for C–OH and 1.22 Å for C=O, respectively, while the angle C–N–C of the pyridine skeleton of EuL corresponds to that of a normal pyridine rather than piperidine. Thus, the proton will locate between O of phenol and N of pyridine in the complex and contribute to keep high planarity of L. Moreover, three nitrate ions coordinated to a Eu^{3+} ion to balance the charge, which confirms that LnL is in the keto–amine form with the coordination number 10. The molecular structures and potential energies for IPT with keto–enol tautomerism in similar molecules with L have been experimentally (LeGourri rec et al., 1998; Hasegawa et al., 1999; Basari c and Wan, 2006) and theoretically (Korth et al., 2002; Li et al., 2017; Wang et al., 2019) demonstrated.

The crystal system of EuL is *triclinic* with a space group of *P*-1. Two molecules form a unit cell (*Z* = 2). These features are consistent with the 100 K data. In contrast, when viewed from the *a*- and *b*-axes, the positions of the atoms in the unit cell are shifted significantly in the *c*-axis direction at 300 K. The length of the unit cell along the *c*-axis is 16.41 Å at 300 K, which is almost 0.30 Å higher than that at 100 K. The unit cell lengths along the *a*- and *b*-axes are almost the same regardless of temperature, whereas the temperature-dependent stretching along the *c*-axis is four times larger than that along the *b*-axis and 40-fold greater than that along the *a*-axis. This trend supports the results of temperature-dependent results of synchrotron XRD measurements (Figure 2). Single crystals of GdL and TbL were prepared and subjected to single-crystal X-ray structural analysis. The results are similar to those for EuL, i.e., the crystal system is *triclinic*, the space group is *P*-1, and the *Z* value is 2. The ligand is tetradentate to the central metal, and three nitrate ions are coordinated to the metal. The molecular and packing structures for TbL and GdL are shown in Supplementary Figures S1 and Supplementary Figures S2, respectively, and the crystal data and bond lengths are shown in Supplementary Table S2. The crystal data and bond lengths for LnL are summarized in Supplementary Table S3. Interestingly, there are two differences between TbL, EuL, and GdL. First,



from the side view of molecules in [Supplementary Figure S1](#), it can be seen that the pyridine ring on one side of TbL is more distorted than those for EuL and GdL. The second difference is in the coordination mode of the nitrate ions. In EuL and GdL, the three nitrate ions are coordinated in a bidentate fashion, whereas in TbL, one of the three nitrate ions is monodentate. In fact, the distance Ln–O (7) between the oxygen atom of the nitrate ion and Tb ion is 3.3 Å, but it is 2.5 Å in the case of EuL and GdL with a difference of about 0.8 Å.

NdL, SmL, DyL, and YbL were also crystallized, and single-crystal X-ray structure analyses were performed ([Supplementary Figures S3–S6](#) and [Supplementary Table S4](#)). The space group of these complexes is also *P*-1. π -electronic systems in TbL, DyL, and YbL distorted resulting in monodentate NO₃[−] coordination, and these crystals contain DMF. Their structural properties correspond to that of TbL. [Table 1](#) summarizes the dihedral angles localized on right and left wings, the dihedral angle between right and left wings (ω_{Left} , ω_{Right} , and ξ , respectively), and the average value of two hydrogen bond distance (r_{HB}) and ionic radii ([Cotton, 2006](#)) for a series of LnL complexes. ω_{Left} differs from ω_{Right} , while every value of the right or left one is equal in NdL, SmL, EuL, and GdL and in TbL, DyL, and YbL. Their molecular structure differences clearly enhanced to the unit cell information, for example, the *c*-axis drastically changes ([Supplementary Table S4](#)). It suggests that L coordinates

without involving ionic radii of Ln, but ionic radii change the coordination number and structures. It was expected that there is some correlation between r_{HB} and the lanthanoid contraction, but no less clear differences have been observed.

2.2 Synchrotron X-ray diffraction

Synchrotron XRD patterns of EuL at various temperatures are shown in [Figure 2](#), where the temperature was decreased from 300 to 90 K and then increased to 300 K again. EuL shows a sharp diffraction pattern at all temperatures. Interestingly, when the *c*-axis of the crystal lattice is not involved, such as for the (010) and (100) planes, no temperature dependences were observed. These peaks associated with (002) and (111) planes, which have a *c*-axis component, shifted to a high angle and became broader at a low temperature. This indicates that the *c*-axis elongates with increasing temperature. From the observed results at 90 and 300 K in [Supplementary Table S1](#), the difference of *c*-axis was 0.31 Å but those of *a*- and *b*-axes were negligibly small. In addition, the XRD pattern obtained by gradually decreasing the temperature from 300 K and then returning to 300 K reproduces the initial 300 K XRD pattern, indicating that the elongation along the *c*-axis is reversible with temperature.

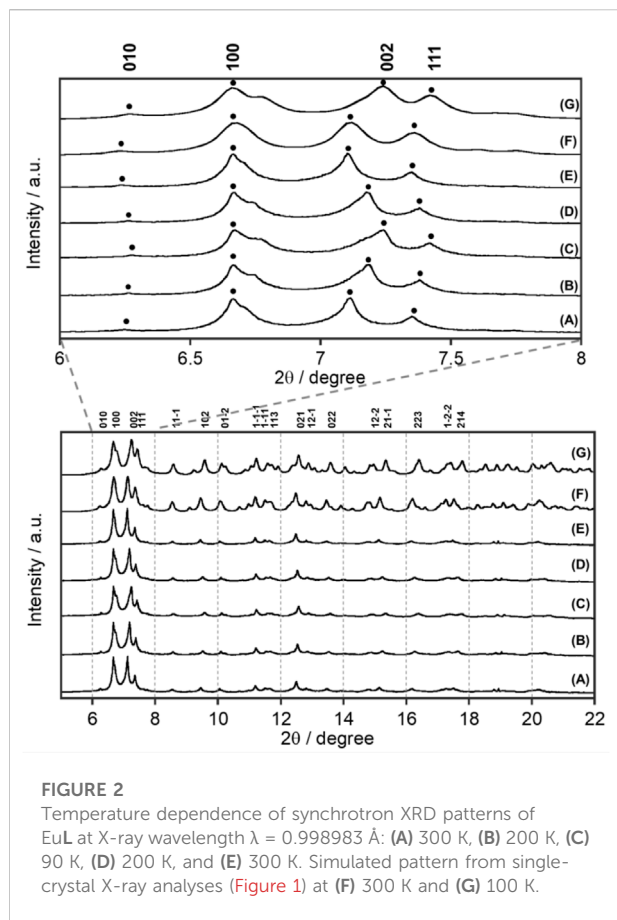
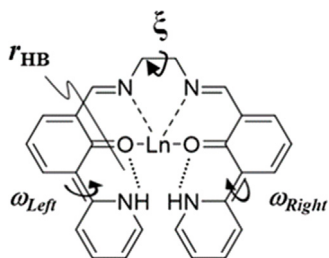


FIGURE 2

Temperature dependence of synchrotron XRD patterns of EuL at X-ray wavelength $\lambda = 0.998983 \text{ \AA}$: (A) 300 K, (B) 200 K, (C) 90 K, (D) 200 K, and (E) 300 K. Simulated pattern from single-crystal X-ray analyses (Figure 1) at (F) 300 K and (G) 100 K.

TABLE 1 Comparison of dihedral angles and ionic radii of LnL (Ln = Nd, Sm, Eu, Gd, Tb, Dy, and Yb). ω_{Left} and ω_{Right} are dihedral angles of aromatic rings crosslinked at C (6)–C (5) and C (21)–C (22), respectively. The ξ value is the dihedral angle between the two π -electronic systems. r_{HB} is the average value of two hydrogen bond distances.

	NdL	SmL	EuL	GdL	TbL	DyL	YbL
Space group	<i>P</i> -1						
$\omega_{Left} / ^\circ$	7.1	7.1	7.1	7.0	8.1	8.3	8.4
$\omega_{Right} / ^\circ$	3.9	4.2	4.3	4.4	2.4	2.5	2.5
$\xi / ^\circ$	0.96	0.63	0.54	0.68	1.70	1.83	1.90
r_{HB}	1.75	1.80	1.81	1.80	1.79	1.81	1.82
Ionic radii/ $\text{\AA}^{(31)}$	0.98	0.96	0.95	0.94	0.92	0.91	0.87



2.3 Thermosensitive/visible-excited luminescence of LnL

Electronic absorption spectra provide considerable information about the electronic state and molecular structure of a molecule. **Supplementary Figure S7** shows electronic absorption spectra of ligand L and EuL, TbL, and GdL complexes in acetonitrile. The ligands show broad bands around 335–430 nm assigned to the $\pi\pi^*$ transitions localized on L. Upon complexation, the band at 335 nm is heavily red-shifted and appears around 380 nm. This is due to $\pi\pi^*$ transitions of the ligand and is independent of the type of metal ion. LnL, the mother skeleton, shows a $\pi\pi^*$ absorption band around 315 nm; thus, the absorption band for LnL is red-shifted by 65 nm. This shift is presumably due to the increased planarity of the electronic system *via* intra-ligand hydrogen bonding. In other words, the electronic state for the ligand is only realized after complexation. The latter band at 430 nm disappeared after the complexation, meaning that it would be an $n\pi^*$ electronic transition localized on the ligand.

Generally, the Gd complex is used as a reference molecule to determine the electronic state for the energy donor electron system. For example, since multidentate ligands such as L take on various conformations in the metal-free state, Gd complexes are commonly used to determine fluorescence and phosphorescence when they have the same structure as ligands of Eu and Tb complexes. **Figure 3C** shows emission spectra of GdL in the solid state at rt and 77 K. GdL exhibits broad emission bands around 440–480 nm and 480–650 nm at rt. The former luminescence band relatively becomes weaker upon cooling and the latter one becomes stronger, which suggests that it is due to the fluorescence band of L. Luminescence lifetime is also suggested from the aforementioned aspect (**Table 2**, **Supplementary Figure S8C,D**). The τ value at $\lambda_{mon} = 470 \text{ nm}$ is estimated to two components: 0.10 (amp. 99.3%) and 1.32 (0.7%) ns at rt and 0.15 (98.0%) and 3.38 (2.0%) at 77 K. On the other hand, the value of $\lambda_{mon} = 540 \text{ nm}$ is estimated as two luminescent components at rt, 3.8 μs (99.9%) and 0.50 ms (0.1%), and three at 77 K, 0.05 ms (58.5%), 0.30 ms (39.5%), and 1.20 ms (2.0%). Thus, this band is phosphorescence of L. The ϕ_{ff} value for GdL at rt was <0.1%; at 77 K, it increased to 44.0%. These results indicate that GdL shows remarkable thermosensitive properties and will discuss the sensitization of the ff-luminescence behavior of other LnL complexes in the following paragraphs. Furthermore, the appearance of the phosphorescence band at ambient temperature means that the heavy metal effect in GdL is efficient.

The solid-state emission spectra of EuL are shown in **Figures 3A,D** at $\lambda_{ex} = 380$ and 400 nm. The bands around 579, 591, 621, 647, and 696 nm at rt are assigned to the $^5D_0 \rightarrow ^7F_0$, $^5D_0 \rightarrow ^7F_1$, $^5D_0 \rightarrow ^7F_2$, $^5D_0 \rightarrow ^7F_3$, and $^5D_0 \rightarrow ^7F_4$ transitions of Eu^{3+} , respectively. The corresponding emission bands at 77 K appear at almost the same wavelength position but become

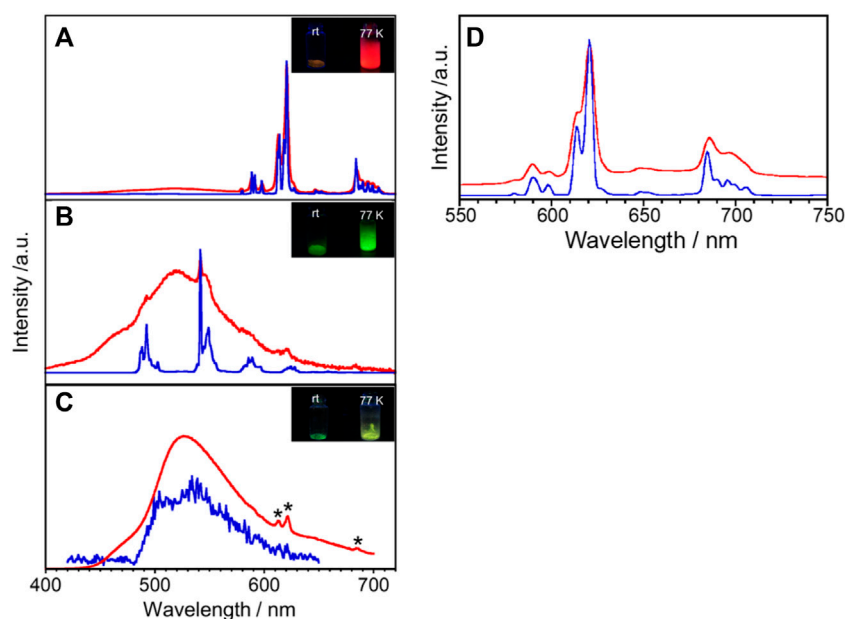


FIGURE 3

Temperature dependence of the solid-state luminescence spectra of (A) EuL, (B) TbL, and (C) GdL at rt (red) and 77 K (blue). $\lambda_{\text{ex}} = 380$ nm, *due to impurity. Inset in (A), (B), and (C): photograph of luminescence of EuL, TbL, and GdL, respectively, at various temperatures. (D) EuL also shows a luminescence band at $\lambda_{\text{ex}} = 400$ nm.

TABLE 2 Luminescence QY and lifetimes of a series of LnL complexes.

	Temp	ϕ_L	$\lambda_{\text{obs}}/\text{nm}$	$\lambda_{\text{ex}}/\text{nm}$	$\lambda_{\text{mon}}/\text{nm}$	$\tau_{\text{av}}/\text{ms}$	τ_1/ms (amp.)	τ_2/ms (amp)	τ_3/ms (amp.)
EuL	rt	1.3%	550–750	365	621	0.23	6.2×10^{-5} (87.6%)	0.17 (11.2%)	0.45 (1.2%)
	77 K	57.3%	550–750	-	-	0.82	0.82 (100%)	-	-
TbL	rt	n.d.	450–700	370	542	-	-	-	-
	77 K	41.6%	450–700	-	-	1.166	0.182 (33.4%)	0.649 (29.2%)	1.456 (37%)
NdL ^a	rt	0.02%	927–1,140	-	-	-	-	-	-
SmL ^a	rt	0.68%	800–1,500	-	-	-	-	-	-
DyL ^a	rt	n.d	-	-	-	-	-	-	-
YbL ^a	rt	0.23%	887–1,152	-	-	-	-	-	-

^aLuminescence QY at 77 K and lifetimes in the NIR wavelength region were not observed due to the apparatus.

sharper than those at rt. The red emission is confirmed visually as shown in Figure 3A. The lowest excitation band position well reproduces the absorption spectrum in acetonitrile (Supplementary Figure S7), indicating that the emission of Eu³⁺ is due to the energy transfer from the ligand. Additionally, EuL exhibits a broad band at 450–575 nm, similar to the spectrum of GdL. As described previously, the emission of Gd complexes is due to fluorescence and phosphorescence of the ligands. In other words, the broad

band for EuL is a ligand-derived emission band with metal-centered sharp bands. The solid-state emission and excitation spectra of TbL are shown in Figure 3B and Supplementary Figure S9. The complex luminescence band around 493, 542, 590, and 628 nm at 77 K are assigned to the ⁵D₄→⁷F₆, ⁵D₄→⁷F₅, ⁵D₄→⁷F₄, and ⁵D₄→⁷F₃ transitions of Tb³⁺, respectively. It also exhibits a broad emission band at 520 nm at rt derived from the ligand, which imposed with a sharp emission band of Tb³⁺. Under the UV irradiation, TbL shows a green emission at rt and 77 K as shown in Figure 3B,

TABLE 3 Photophysical parameters of EuL in the solid state. (^a: $\lambda_{\text{ex}} = 380$ nm, $\lambda_{\text{mon}} = 583\text{--}603$ nm;^b: $\lambda_{\text{ex}} = 380$ nm, and $\lambda_{\text{mon}} = 550\text{--}750$ nm).

	Temp	I_{MD}^{a}	$I_{\text{tot}}^{\text{b}}$	$\tau_{\text{av}}/\text{s}$	$k_{\text{R}}/\text{s}^{-1}$	$k_{\text{NR}}/\text{s}^{-1}$	φ_{Ln}	η_{EnT}
EuL	rt	9.7×10^{-4}	1.3×10^{-2}	2.3×10^{-4}	662	3,685	0.15	0.085
	77 K	0.053	0.57	8.2×10^{-4}	531	687	0.43	≈ 1.0

inset. However, the origin of the luminescence differs; the green luminescence at rt was ligand-dominated, while that was due to the ff transitions at 77 K.

Luminescence profiles, lifetimes, and QY for a series of LnL complexes are shown in **Supplementary Figure S8** and **Table 2**. The φ_{L} value for EuL at 77 K (57.3%) is about 40 times higher than that at rt (1.3%). Such temperature-dependent Eu complexes have rarely been reported. Under the molecular design concept which having an absorption band at the visible wavelength region, it unexpectedly accelerates a drastic spectral change in Eu emission by temperature stimuli. The luminescence lifetime for EuL at 621 nm at 77 K is 0.82 ms as a single component. On the other hand, at rt, the luminescence lifetime for EuL is analyzed as three components, 6.2×10^{-5} , 0.17, and 0.45 ms at 621 nm, meaning that various transitions overlap at this wavelength as described previously (**Figure 3A**). The φ_{L} value for TbL at rt could not be estimated due to being negligibly weak. Remarkably, the φ_{L} value for TbL at 77 K increases up to 46.1%. Two luminescence components for TbL at rt were estimated as 0.091 and 0.661 ms monitored at 542 nm. From the comparison of luminescence lifetimes of GdL, the shorter-lifetime components for EuL and TbL are assumed to be due to $\pi\pi^*$ transitions in the ligand.

Quantitative energy relaxation can be discussed by using aforementioned luminescence properties of the Eu complex, since the electronic transitions of Eu^{3+} independently appear in their magnetic dipole transitions and electric transitions. The luminescence efficiency (Bünzli et al., 2007) of Eu^{3+} sensitized by the ligand (φ_{L} is determined by the triplet yield of the ligand (φ_{ISC}) (El-Sayed, 1963), the efficiency of the energy transfer (η_{EnT}), and the efficiency of the metal-centered luminescence (φ_{Ln}) are expressed as follows:

$$\varphi_{\text{L}} = \varphi_{\text{ISC}} \times \eta_{\text{EnT}} \times \varphi_{\text{Ln}}, \quad (1)$$

$$\varphi_{\text{Ln}} = k_{\text{R}} / (k_{\text{R}} + k_{\text{NR}}) = k_{\text{R}} \times \tau_{\text{av}}, \quad (2)$$

$$k_{\text{R}} = A_{\text{MD},0} \times n^3 \times (I_{\text{tot}} / I_{\text{MD}}). \quad (3)$$

The photophysical properties of EuL are calculated using **Eqs 1–3**, where $\varphi_{\text{ISC}} = 1$ (Bünzli et al., 2007; Hasegawa et al., 2018) and $n = 1.5$ for the solid state and k_{R} and k_{NR} are radiative and non-radiative decay rates, respectively. $A_{\text{MD},0}$ is a constant relating to the spontaneous emission probability for the ${}^5\text{D}_0 \rightarrow {}^7\text{F}_0$ of Eu^{3+} in vacuum (14.65 s^{-1}). I_{tot} and I_{MD} are integrated luminescence intensity of the total luminescence of

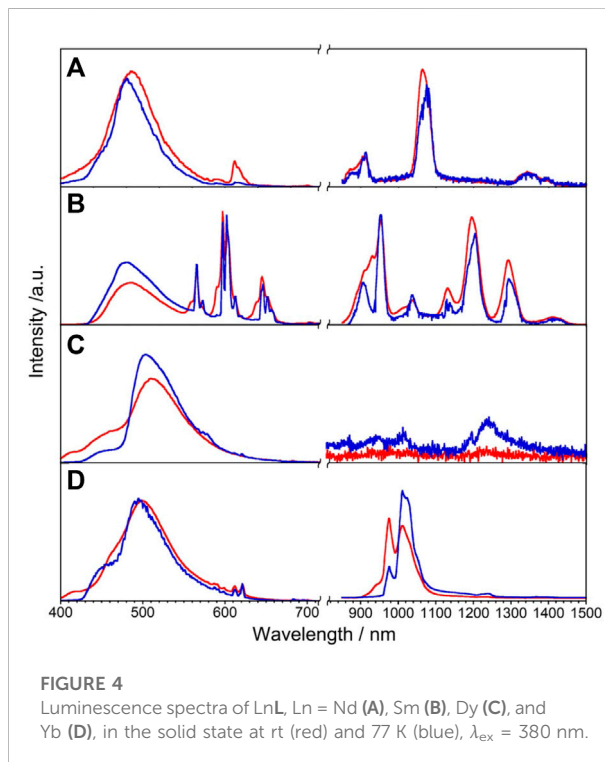
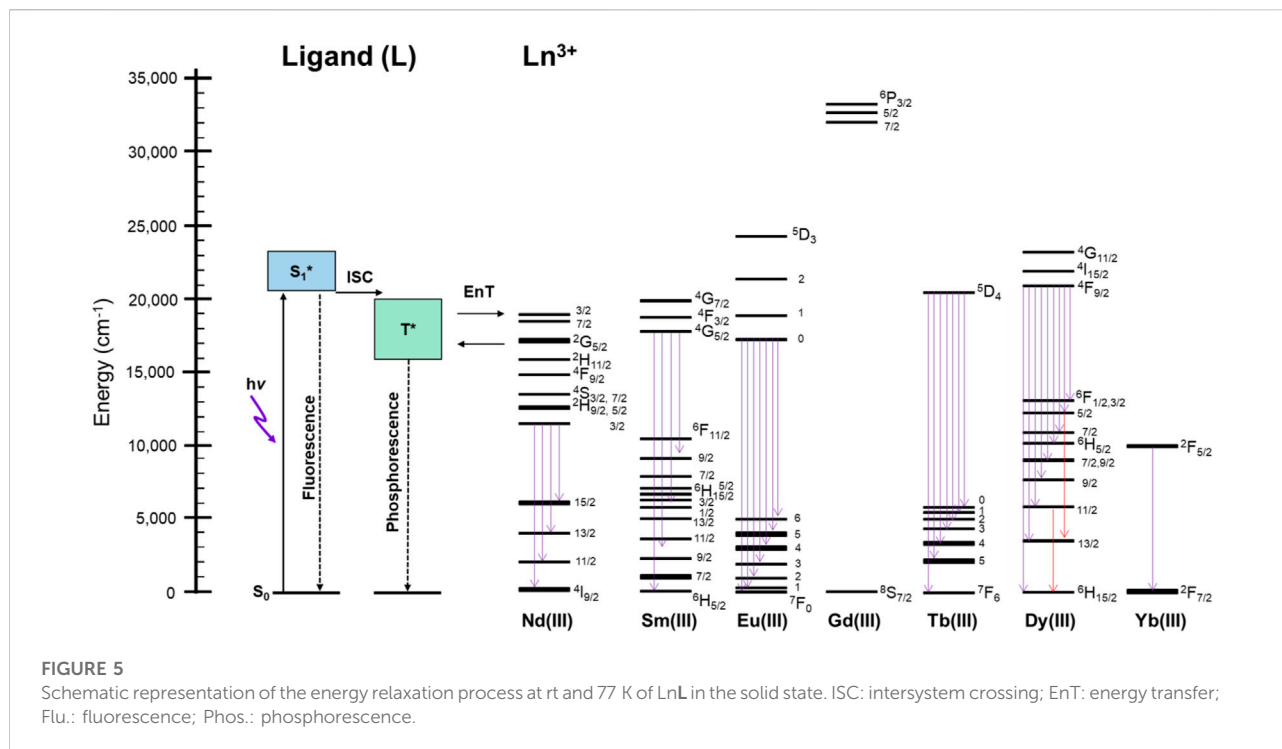


FIGURE 4 Luminescence spectra of LnL, Ln = Nd (A), Sm (B), Dy (C), and Yb (D), in the solid state at rt (red) and 77 K (blue), $\lambda_{\text{ex}} = 380$ nm.

EuL (550–750 nm) and the region of ${}^5\text{D}_0 \rightarrow {}^7\text{F}_1$ (583–603 nm), respectively, and are determined from their spectral area recorded on an absolute emission quantum yield spectrometer C9920-02. The calculated results are shown in **Table 3**. It is worth noting that the η_{EnT} value shows obvious temperature dependence, for example, the values at rt and 77 K are 0.084% and $\approx 100\%$, respectively.

We expected that the energy donor level of L will also be efficient to sensitize NIR luminescence of Nd, Sm, Dy, and Yb via the intramolecular energy transfer. The luminescence spectra of LnL (Ln = Nd, Sm, Dy, and Yb) at rt and 77 K are shown in **Figure 4**. NdL clearly shows emission bands around 911, 1,063, and 1,340 nm at rt, which are assigned to ${}^4\text{F}_{3/2} \rightarrow {}^4\text{I}_j$ ($J = 9/2, 11/2,$ and $13/2$, respectively) transitions of Nd^{3+} . The band positions and relative intensities are stable at 77 K. The broad band at a similar position observed at 420 nm of GdL also appeared in the case of NdL as $\pi\pi^*$ transitions. SmL shows emission bands around 951, 1,037, 1,132, 1,191, and 1,292 nm assigned to the ${}^4\text{G}_{5/2} \rightarrow {}^6\text{F}_j$ ($J = 5/2, 7/2, 9/2, 11/2,$ and $13/2$, respectively)



transitions of Sm^{3+} , accompanied with $\pi\pi^*$ luminescence bands. DyL shows luminescence bands around 570 nm in the visible region and around 1,010–1,190 nm in the NIR region, attributed to the ${}^4\text{F}_{9/2} \rightarrow {}^6\text{H}_{7/2}$ and ${}^4\text{F}_{9/2} \rightarrow {}^6\text{H}_{5/2}$ transitions, respectively. In general, Dy^{3+} shows emission bands in the wavelength region of visible-NIR (around 475, 570, 660, 750, 1,000, 1,180, 1,270, and 1,400 nm), but DyL does not show these bands because of the superimposition between $\pi\pi^*$ luminescence band and ff ones. YbL shows the emission band at 970–1,080 nm assigned to the ${}^2\text{F}_{5/2} \rightarrow {}^2\text{F}_{7/2}$ transition of Yb^{3+} . The split band shape of YbL shows temperature dependence and becomes shaper at 77 K than at rt. The absolute luminescence quantum yields ff at rt in the NIR region for NdL, SmL, DyL, and YbL are 0.02%, 0.68%, $<10^{-6}\%$, and 0.23%, respectively.

Figure 5 shows the schematic representation for the explanation of the thermosensitive energy relaxation for LnL. These complexes take the photoexcited donor state by visible light. The fluorescence and phosphorescence bands of GdL with peak position at 460–470 nm, respectively, appear mostly in the similar position with relatively large band width (Figure 3). Then, the exciton at T^* via intersystem crossing undergoes energy relaxation due to phosphorescence and transfers photoexcited energy to the metal. This is based on the fact that phosphorescence and ff emission are observed simultaneously. Interestingly, these complexes with Nd, Sm, Eu, Tb, Dy, and Yb also retain the ligand-centered $\pi\pi^*$ luminescence at rt and 77 K with their ff emission. As described previously, the ligand emission at rt is more dominant in the case of TbL than in

the case of EuL because the acceptor level for Tb^{3+} is higher in energy than the acceptor level for Eu^{3+} , and then the ligand emission strongly appears more than ff emission of Tb^{3+} at rt and *vice versa* at 77 K. In particular, EuL obviously exhibits the temperature dependences in luminescence spectra. The multiphonon mechanism is one of the possibilities to enhance such temperature dependence of ff emissions in Ln complexes (Kreidt et al., 2018). Actually, the stretching vibration of N–H was observed around $3,100\text{ cm}^{-1}$ in EuL and TbL originated from L from the measurement of FT-IR (ATR method) as shown in Supplementary Figure S10. The band position of EuL, for example, at 621 nm ($16,100\text{ cm}^{-1}$) corresponds to the five times of N–H vibration, which will contribute to the temperature dependence of Eu emission with L. Thus, the ligand L does not only sensitize the ff emission at visible light but also results in both ligand-/Ln-centered emission or their selectivity at various temperatures due to the energy levels of donor and acceptor levels.

3 Conclusion

Yellowish complexes, LnL (Ln = Nd, Sm, Eu, Gd, Tb, Dy, and Yb), are sufficient electronic structures as visible-light-excited visible dual luminescence compounds taken into account the π -electronic system coplanarity through intramolecular hydrogen bonding. Molecular and packing structures for a series of LnL complexes take isostructure. L coordinates to Ln^{3+} as a

tetradentate ligand. The intramolecular hydrogen bonds through keto–amine and enol–imine isomerization keep the molecular planarity of the ligand moiety, which results that the electronic absorption bands appear at the visible region. Single-crystal X-ray structural analysis of the series of Ln complexes was also performed. A significant change in the crystal structure occurs after gadolinium. Synchrotron XRD and single-crystal X-ray structural analysis show temperature dependence in the *c*-axis direction, but no influence of the temperature dependence was observed in the excited state of **L**.

TbL exhibits ff emission and ligand emission simultaneously with temperature dependence based on the thermal equilibrium between energy donor and acceptor levels. The absolute luminescence quantum yields for EuL at 77 K are much higher than those at rt, and the intramolecular energy transfer was quantitatively discussed by their luminescence lifetimes. The QYs of ff emissions of EuL also show drastic temperature dependence due to the multiphonon effect relating to the N–H vibration of **L**. The band positions of $\pi\pi^*$ emission of GdL support to explain the aforementioned phenomena from the viewpoint of the intramolecular energy transfer mechanism. The ligand **L** also acts as an energy donor to induce NIR luminescence of several kinds of Ln³⁺. It was found that these cases show metal selectivity to Dy and thermo-sensitivity. Thus, it is surely expected that a series of LnL complexes are applicable to luminescent thermo-sensors, especially toward self-calibrated thermometers (Rocha et al., 2016), which have never used the excitation light in the visible region.

4 Materials and methods

4.1 Materials

The commercially available chemicals were of analytical reagent grade and were used without further purification: 3-bromosalicylaldehyde, tributyl (2-pyridyl)tin, tetrakis (triphenylphosphine)palladium (0), dry ethylenediamine, and Ln (NO₃)₃·6H₂O. All other starting materials were of analytical grade, obtained from commercial sources, and were used without further purification.

4.2 Synthesis of 6,6'-(1E,1'E)-(ethane-1,2-diylbis(azaneylyliden-e))bis(methaneylylidene))bis(2-(pyridine-2-yl)phenol) (II: **L**)

2-Hydroxy-3-(2-pyridinyl)-benzaldehyde(I) was synthesized through the process already reported in Honda and Arai (2016). Yield: 460 mg (47%); ¹H-NMR (500 MHz, CDCl₃) δ 10.62 (t, J = 14.9 Hz, 1H), 8.56 (td, J = 3.3, 1.7 Hz, 1H), 8.06 (dd, J = 7.4, 1.7 Hz, 1H), 7.97 (d, J = 8.0 Hz, 1H), 7.86–7.92 (m, 2H), 7.32–7.35 (m, 1H), and 7.00 (t, J = 7.7 Hz, 1H).

L was synthesized from two equivalents of (I) bridged with an ethylenediamine and obtained as a yellowish powder according to Hasegawa et al. (2014). Yield: 234 mg (52%); ¹H-NMR (500 MHz, CDCl₃) δ 8.67 (d, J = 4.0 Hz, 2H), 8.53 (s, 2H), 8.05 (d, J = 8.0 Hz, 2H), 7.94 (d, J = 7.4 Hz, 2H), 7.74–7.77 (m, 2H), 7.23 (ddd, J = 7.4, 5.2, 1.1 Hz, 2H), 6.98 (t, J = 7.4 Hz, 2H), and 3.99 (t, J = 14.9 Hz, 4H).

4.3 Synthesis of Ln complexes with **L** (III: LnL) (EuL, TbL, GdL, NdL, SmL, DyL, and YbL)

L (50.2 mg, 0.118 mmol) was dissolved in 50 ml of methanol and stirred with a solution of Eu(NO₃)₃·6H₂O (52.79 mg, 0.118 mmol) in 5 ml of methanol at rt for 3 h. The mixture was passed through a membrane filter, and LnL was obtained as a yellowish powder. Yield: EuL (72 mg, 95%), GdL (16 mg, 21%), TbL (74 mg, 80%), NdL (78 mg, 85%), SmL (74 mg, 79%), DyL (78.7 mg, 77%), and YbL (78 mg, 82%). Elemental analyses for EuL: C₂₆H₂₂N₇O₁₁Eu (Calcd.: C 41.07; H 2.92; N 12.89. Found: C 41.1; H 2.95; N 12.76); GdL: C₂₆H₂₂N₇O₁₁Gd (Calcd.: C 40.78; H 2.90; N 12.80. Found: C 40.73; H 2.92; N 12.62); TbL: C₂₆H₂₂N₇O₁₁Tb (Calcd.: C 40.69; H 2.89; N 12.78. Found: C 40.74; H 2.94; N 12.65); NdL: C₂₆H₂₂N₇O₁₁Nd (Calcd.: C 41.49; H 2.95; N 13.03. Found: C 41.54, H 2.92, N 12.89); SmL: C₂₆H₂₂N₇O₁₁Sm (Calcd.: C 41.15, H 2.92, N 12.92. Found: C 41.09, H 2.86, N 12.82); DyL: C₂₆H₂₂N₇O₁₁Dy (Calcd.: C 40.50, H 2.88, N 12.72. Found: C 40.46, H 2.86, N 12.42); and YbL: C₂₆H₂₂N₇O₁₁Yb (Calcd.: C 39.96, H 2.84, N 12.55. Found: C 39.93, H 2.78, N 12.37).

4.4 Apparatus

Elemental analyses (C, H, and N) were performed using a vario EL (Elementar Analysensysteme GmbH Co.). ¹H-NMR spectra were collected on a JEOL JNM-ECP 500. UV spectra and luminescence spectra were recorded on a Shimadzu UV-3600S and a Horiba Jobin Yvon Fluorolog 3-22, respectively. Absolute luminescence quantum yield values were measured using a Hamamatsu Photonics K.K. C9920-02 for the UV-vis wavelength region and C13534 for NIR. Structural analyses of a series of LnL complexes were performed using a Rigaku Synergy S and XtaLAB mini II, Rigaku Oxford diffractometer with Mo K α radiation (λ = 0.71073 Å). The structures were solved by direct methods and refined on *F*² by a full-matrix least-squares method using the SHELXTL-97 program: CCDC 2144933 (at 90 K) and 2144934 (at 300 K) for EuL, 2144935 for GdL, 2144936 for TbL, 2144931 for NdL, 2144932 for SmL, 2144937 for DyL, and 2144938 for YbL. Synchrotron X-ray diffraction data were collected at the beam line BL02B2 (λ = 0.998983 Å) in SPring-8. The sample was

held in a glass capillary (Markröhrchenaus Glas, 0.3 mm, Hilgenberg Co.)

Data availability statement

The datasets presented in this study can be found in online repositories. The names of the repository/repositories and accession number(s) can be found at: <https://www.ccdc.cam.ac.uk/structures/—2144931—2144938>.

Author contributions

MH and NM conceived the study. HO, JK, MY, TM, and YT performed the synthesis and crystallization of Ln complexes and measured their photophysical properties. AI, YY, and YO checked the reproducibility of these photophysical properties. KG evaluated the elemental analysis and the way of syntheses. MK and DS experimentally determined the crystal structures.

Funding

This work was supported by JSPS KAKENHI, Japan, for Scientific Research on Innovative Areas “Soft Crystals (Area Number 2903),” under Grant Nos. 17H06366 (MK) and 17H06374 (MH); the Grant-in-Aid for Early-Career Scientists,

References

- An, B.-L., Zhang, N., Cheah, K.-W., and Pan, Q.-Y. (2008). High yield luminescence of a novel europium complex by excimer excitation and f-f absorption of Eu³⁺. *J. Alloys Compd.* 458, 457–461. doi:10.1016/j.jallcom.2007.04.003
- Andreadis, E., Demadrille, R., Imbert, D., Pécaut, J., and Mazzanti, M. (2009). Remarkable tuning of the coordination and photophysical properties of lanthanide ions in a series of tetrazole-based complexes. *Chem. Eur. J.* 15, 9458–9476. doi:10.1002/chem.200900912
- Aquino, L. E. D. N., Barbosa, G. A., Ramos, J. D. L., Giese, S. O. K., Santana, F. S., Hughes, D. L., et al. (2021). Seven-coordinate Tb³⁺ complexes with 90% quantum yields: High-performance examples of combined singlet- and triplet-to-Tb³⁺ energy-transfer pathways. *Inorg. Chem.* 60, 892–907. doi:10.1021/acs.inorgchem.0c03020
- Basarić, N., and Wan, P. (2006). Excited state proton transfer (ESPT) from phenol to nitrogen and carbon in (2-hydroxyphenyl)pyridines. *Photochem. Photobiol. Sci.* 5, 656–664. doi:10.1039/b600826g
- Bender, J. L., Corbin, P. S., Fraser, C. L., Metcalf, D. H., Richardson, F. S., Thomas, E. L., et al. (2002). Site-isolated luminescent europium complexes with polyester macroligands: Metal-centered heteroarm stars and nanoscale Assemblies with labile block junctions. *J. Am. Chem. Soc.* 124, 8526–8527. doi:10.1021/ja0261269
- Binnemans, K. (2015). Interpretation of europium(III) spectra. *Coord. Chem. Rev.* 295 (4), 1–45. doi:10.1016/j.ccr.2015.02.015
- Bünzli, J.-C. G., Comby, S., Chauvin, A.-S., and Vandevyver, C. D. B. (2007). New opportunities for lanthanide luminescence. *J. Rare Earths* 25, 257–274. doi:10.1016/S1002-0721(07)60420-7
- Bünzli, J.-C. G., Froidevaux, P., and Harrowfield, J. M. (1993). Complexes of lanthanoid salts with macrocyclic ligands. 41. Photophysical properties of lanthanide dinuclear complexes with p-tert-butylcalix[8]arene. *Inorg. Chem.* 32, 3306–3311. doi:10.1021/ic00067a019

under Grant No. 20K15041 (HO); Aoyama Gakuin University Research Institute’s “Early Eagle” grant program for promotion of research by early career researchers (HO); the Tokuyama Science Foundation, Japan (HO); and the Cooperative Research Program of “Network Joint Research Center for Materials and Devices,” under Grant Nos. 20201320, 20211314, and 20221164 (MH and HO).

Conflict of interest

There are no conflicts to declare.

Publisher’s note

All claims expressed in this article are solely those of the authors and do not necessarily represent those of their affiliated organizations, or those of the publisher, the editors, and the reviewers. Any product that may be evaluated in this article, or claim that may be made by its manufacturer, is not guaranteed or endorsed by the publisher.

Supplementary material

The Supplementary Material for this article can be found online at: <https://www.frontiersin.org/articles/10.3389/fchem.2022.1047960/full#supplementary-material>

- Chen, F.-F., Bian, Z.-Q., Liu, Z.-W., Nie, D.-B., Chen, Z.-Q., and Huang, C.-H. (2008). Highly efficient sensitized red emission from europium (III) in Ir–Eu bimetallic complexes by 3MLCT energy transfer. *Inorg. Chem.* 47, 2507–2513. doi:10.1021/ic701817n
- Cotton, S. (2006). in *Lanthanide and actinide Chemistry* (A Wiley textbook series, Inorganic Chemistry), 9–22. Chap. 2.
- Deiters, E., Song, B., Chauvin, A., Vandevyver, C., Gumy, F., and Bünzli, J.-C. G. (2009). Luminescent bimetallic lanthanide bioprobes for cellular imaging with excitation in the visible-light range. *Chem. Eur. J.* 15, 885–900. doi:10.1002/chem.200801868
- Deun, R. V., Nockemann, P., Fias, P., Hecke, K. V., Meervelt, L. V., and Binnemans, K. (2005). Visible light sensitisation of europium(III) luminescence in a 9-hydroxyphenal-1-one complex. *Chem. Commun.* 5, 590–592. doi:10.1039/b414703k
- Divya, V., Biju, S., Varma, R. L., and Reddy, M. L. P. (2010). Highly efficient visible light sensitized red emission from europium tris[1-(4-biphenoyl)-3-(2-fluoroyl)propanedione](1, 10-phenanthroline) complex grafted on silicananoparticles. *J. Mater. Chem.* 20, 5220–5227. doi:10.1039/c0jm00588f
- El-Sayed, M. A. (1963). Spin–orbit coupling and the radiationless processes in nitrogen heterocyclics. *J. Chem. Phys.* 38, 2834–2838. doi:10.1063/1.1733610
- Francis, B., Nolasco, M. M., Brandão, P., Ferreira, R. A. S., Carvalho, R. S., Cremona, M., et al. (2020). Efficient visible-light-excitable Eu³⁺ complexes for red organic light-emitting diodes. *Eur. J. Inorg. Chem.* 2020, 1260–1270. doi:10.1002/ejic.202000027
- Gu, Y.-J., and Yan, B. (2013). Europium (III) complex functionalized Si-MCM-41 hybrid materials with visible-light-excited luminescence. *Inorganica Chim. Acta* 408, 96–102. doi:10.1016/j.ica.2013.09.008

- Hasegawa, M., Yamada, Y., Kumagai, K., and Hoshi, T. (1999). Electronic structure of 2, 6-bis{N-(2-hydroxyphenyl)iminoethyl}-4-methylphenol. *Z. für Naturforsch. B* 54b, 929–939. doi:10.1515/znb-1999-0717
- Hasegawa, M., and Ohmagari, H. (2020). Helicate lanthanide complexes: The luminescent elements. *Chem. Lett.* 49 (7), 845–854. doi:10.1246/cl.200184
- Hasegawa, M., Ohtsu, H., Kodama, D., Kasai, T., Sakurai, S., Ishii, A., et al. (2014). Luminescence behaviour in acetonitrile and in the solid state of a series of lanthanide complexes with a single helical ligand. *New J. Chem.* 38, 1225–1234. doi:10.1039/c3nj00910f
- Hasegawa, Y., Ishii, A., Inazuka, Y., Yajima, N., Kawaguchi, S., Sugimoto, K., et al. (2018). The enhanced intramolecular energy transfer and strengthened energy transfer of a stable helical Eu complex in ionic liquids. *Molecules* 23, 55. doi:10.3390/molecules23020055
- He, P., Wang, H. H., Liu, S. G., Shi, J. X., Wang, G., and Gong, M. L. (2009). Visible-light excitable europium(III) complexes with 2, 7-positional substituted carbazole group-containing ligands. *Inorg. Chem.* 48, 11382–11387. doi:10.1021/ic901210c
- He, P., Wang, H. H., Yan, H. G., Hu, W., Shi, J. X., and Gong, M. L. (2010). A strong red-emitting carbazole based europium(III) complex excited by blue light. *Dalton Trans.* 39, 8919–8924. doi:10.1039/c0dt00424c
- Honda, T., and Arai, T. (2016). Control of photocleavage reaction by intramolecular hydrogen bonding in (3-benzoxazolyl-2-hydroxy-5-methylphenyl)methyl acetate. *Bull. Chem. Soc. Jpn.* 89, 254–256. doi:10.1246/bcsj.20150347
- Jiang, L., Wu, J., Wang, G., Ye, Z., Zhang, W., Jin, D., et al. (2010). Development of a visible-light-sensitized europium complex for time-resolved fluorometric application. *Anal. Chem.* 82 (6), 2529–2535. doi:10.1021/ac100021m
- Kasprzycka, E., Victor, A. T., Amirkhanov, V. M., Jerzykiewicz, L., Malta, O. L., Legendziewicz, J., et al. (2017). Contribution of energy transfer from the singlet state to the sensitization of Eu³⁺ and Tb³⁺ luminescence by sulfonylamidophosphates. *Chem. Eur. J.* 23, 1318–1330. doi:10.1002/chem.201603767
- Korth, H.-G., Heer, M. I. D., and Mulder, P. (2002). A DFT study on intramolecular hydrogen bonding in 2-substituted phenols: Conformations, enthalpies, and correlation with solute parameters. *J. Phys. Chem. A* 106, 8779–8789. doi:10.1021/jp025713d
- Kreidt, E., Kruck, C., and Seitz, M. (2018). “Nonradiative deactivation of lanthanide luminescence by multiphonon relaxation in molecular complexes”. Editors J.-C. G. Bünzli and V. K. Pecharski, 53, 35–79. *Handb. Phys. Chem. Rare Earths*
- LeGourriérec, D., Kharlanov, V., Brown, R. G., and Rettig, W. (1998). Excited-state intramolecular proton transfer (ESIPT) in 2-(2'-hydroxyphenyl)pyridine and some carbon-bridged derivatives. *J. Photochem. Photobiol. A Chem.* 117, 209–216. doi:10.1016/S1010-6030(98)00328-1
- Li, Y., Wen, K., Feng, S., Yuan, H., An, B., Zhu, Q., et al. (2017). Tunable excited-state intramolecular proton transfer reactions with N H or O H as a proton donor: A theoretical investigation. *Spectrochimica Acta Part A Mol. Biomol. Spectrosc.* 187, 9–14. doi:10.1016/j.saa.2017.06.019
- Ning, Y., Zhu, M., and Zhang, J.-L. (2019). Near-infrared (NIR) lanthanide molecular probes for bioimaging and biosensing. *Coord. Chem. Rev.* 399, 213028. doi:10.1016/j.ccr.2019.213028
- Parker, D., Fradgley, J. D., and Wong, K.-L. (2021). The design of responsive luminescent lanthanide probes and sensors. *Chem. Soc. Rev.* 50, 8193–8213. doi:10.1039/d1cs00310k
- Rocha, J., Brites, C. D. S., and Carlos, L. D. (2016). Lanthanide organic framework luminescent thermometers. *Chem. Eur. J.* 22, 14782–14795. doi:10.1002/chem.201600860
- Sun, L., Wang, Z., Zhang, J. Z., Feng, J., Liu, J., Zhao, Y., et al. (2014). Visible and near-infrared luminescent mesoporous titania microspheres functionalized with lanthanide complexes: Microstructure and luminescence with visible excitation. *RSC Adv.* 4, 28481. doi:10.1039/C4RA03781B
- Wang, W., Marshall, M., Collins, E., Marquez, S., Mu, C., Bowen, K. H., et al. (2019). Intramolecular electron-induced proton transfer and its correlation with excited-state intramolecular proton transfer. *Nat. Commun.* 10, 1170. doi:10.1038/s41467-019-09154-5
- Werts, M. H. V., Duin, M. A., Hofstraat, J. W., and Verhoeven, J. W. (1999). Bathochromicity of Michler's ketone upon coordination with lanthanide(III) β-diketonates enables efficient sensitization of Eu³⁺ for luminescence under visible light excitation. *Chem. Commun.* 9, 799–800. doi:10.1039/a902035g
- Xu, L., Feng, L., Han, Y., Jing, Y., Xian, Z., Liu, Z., et al. (2014). Supramolecular self-assembly enhanced europium(III) luminescence under visible light. *Soft Matter* 10, 4686–4693. doi:10.1039/c4sm00335g
- Yang, C., Fu, L., Wang, Y., Zhang, J., Wong, W., Ai, X., et al. (2004). A highly luminescent europium complex showing visible-light-sensitized red emission: Direct observation of the singlet pathway. *Angew. Chem. Int. Ed.* 43, 5010–5013. doi:10.1002/anie.200454141
- Zhang, D., Zhang, Y., Wang, Z., Zheng, Y., Zheng, X., Gao, L., et al. (2021). Biodegradable film enabling visible light excitation of Hexanuclear Europium(III) complex for various applications. *J. Lumin.* 229, 117706. doi:10.1016/j.jlumin.2020.117706
- Zhang, L., Liu, H., Zhang, R., Mu, Y., Qian, D., and Feng, X. (2005). Fabrication and characterization of luminescent self-assembled thin films of europium complex. *Colloids Surfaces A Physicochem. Eng. Aspects* 257–258, 401–404. doi:10.1016/j.colsurfa.2004.10.080
- Zhang, L., Tian, L., Ye, Z., Song, B., and Yuan, J. (2013). Preparation of visible-light-excited europium biolabels for time-resolved luminescence cell imaging application. *Talanta* 108, 143–149. doi:10.1016/j.talanta.2013.02.065